ULTRA-LONG PERIOD SEISMIC SIGNALS AND CYCLIC DEFLATION COINCIDENT WITH ERUPTIONS AT SANTIAGUITO VOLCANO, GUATEMALA

By

Richard William Sanderson

Submitted in Partial Fulfillment
of the Requirements for the Degree of
Master of Science in Geophysics (Solid Earth)

New Mexico Institute of Mining and Technology
Socorro, New Mexico

May 2010

ABSTRACT

Broadband seismic observations made near the active vent at Santiaguito provide constraints on changing pressures inside the edifice. During January 2009 we recorded episodic ultra-long period signals (ULPs, > 30 s) that were coincident with eruptive activity centered on the active El Caliente vent. These signals lasted 2-5 minutes and corresponded to depressurization of a volume beneath the dome. Coincident shorter-period seismic signals (> 0.5 Hz) appeared to be associated with shallow level pyroclastic emissions and dome surface motions. These shorter period signals varied significantly from event to event, unlike the ULP waveforms, which were self similar. Unlike the short period signals, the ULPs were only recorded on the horizontal channels of 3 stations that were within 1.1 km of the vent indicating that they were a result of long-period rotation rather than horizontal translation. Initial ULP source locations derived from horizontal particle motions point to the north-western part of El Caliente 150 m from the vent axis, the general locus of activity until a flank collapse in 1989/1990. We modeled the ULP signal as a Mogi source and solved for three dimensional location and equivalent source strength. Through analysis of 76 events, we identify a mean Mogi source that is 200 m west of and 250 m beneath the centre of the vent with the peak volume changes accompanying eruptions ranging from 125 to 1825 m^3. These inferred volume losses coincide with the onset of gas venting and/or explosive eruptions at the surface of Caliente. Based upon these observations we develop a model is to describe the pre-eruptive, eruptive and inter-eruptive physical processes occurring on at the surface and inside Santiaguito.

ACKNOWLEDGEMENTS

Special thanks go to my advisor Jeffrey B. Johnson for providing inspiration and guidance as well as to my other committee members Richard C. Aster and Jonathan M. Lees.

I am grateful for support from INSIVUMEH (through G. Chigna), the Policía Nacional Civil de Guatemala and the Instituto Guatemalteco de Turismo (through C. Barrio), G.P. Waite, K. Brill, J. Anderson, C. Forbes, E. Lopez, A. Miller, J. Lyons, J. Silverman and R. Wolf in addition to S. Every, O. Marcillo and J. Normand for assistance with data collection during January 2007. Also appreciated is the helpful discussion and comments from N. Varley, K. Tsukui and G. Divine.

This work was possible through financial support from NSF EAR 0738802, NSF EAR 0838562 and NSF PIRE 0530109.

TABLE OF CONTENTS

Page

LIST OF FIGURES

Figure **Page**

INTRODUCTION

Subsurface volcanic bodies that inflate and deflate over varying timescales have been studied using in-situ tilt meters and remote sensing tools such as electronic distance meters and InSAR that measure surface deformation (e.g. Iguchi et al., 2008; Tiampo et al., 2000; Amelung, 2000). The broadband seismometer has also been used to measure deformations at volcanoes such as Stromboli (Wielandt and Forbriger, 1999), Anatahan (Wiens et al., 2005), Meakan-dake (Aoyama and Oshima, 2008) and Aso (Kawakatsu et al., 2000) and has led to identification of magma reservoirs and activity of hydrothermal systems. The sensitivity of a broadband seismometer's horizontal channels to rotational strains provides a useful tool for near-vent monitoring of volcanoes. Pseudo-tilt extracted from seismometers may be used to monitor surface deformation and can be related to surface eruptions of material (Wielandt and Forbriger, 1999). Such cyclic tilt sequences have been observed during several dome building eruptions e.g. Soufrière Hills volcano, Montserrat where there is deflation during extrusion (Costa et al., 2007) and Merapi, Indonesia, which inflates during extrusion (Voight et al., 2000). Deformation periods range from several seconds to decades and have been attributed to changing conduit dimensions, varying flow rates, and upper conduit pressurization (e.g., Costa et al., 2007 and Wylie et al., 1999 for more thorough reviews). Seismic pseudo-tilt can be used to monitor deformations over time scales of seconds to hours (Wiens et al., 2005).

Several studies have focused on the dynamics of the ongoing Santiaguito eruptions, which has persisted with minor fluctuations for the last 87 years building a 1.1 km^3 dacite lava dome (Rose, 1973). These studies have focused on visual observations

(Johnson et al., 2008; Bluth and Rose, 2004), thermal observations (Sahetapy-Engel et al., 2008), gas remote sensing (Yamamoto et al., 2008), and seismo-acoustic observations (Johnson et al., 2004). These field observations have provided insight into the mechanism of repeat eruptive events from volcanic domes (e.g., Barmin et al., 2002).One existing eruptive model suggests that that gas preferentially escapes the magma along the surface between it and the encompassing conduit walls (Sahetapy-Engel et al., 2008; Bluth and Rose, 2004; Gonnermann and Manga, 2003). Magma ascent beneath a viscous plug causes stick-slip behaviour and consequently critical depressurization of gasses resulting in the observed eruptions. Another model considers the eruptive mechanism in more detail by modeling the surface of the active dome as a 'pad' that shifts up and down as gas reaches a critical pressurization level beneath it (Johnson et al, 2008). Subsequent modeling using a single event showed that additional features may include precursory gas venting and co-eruptive decompression of the dome followed by a slow return to equilibrium (Johnson et al, 2009). This paper further analyses the nature of cyclic decompression and recompression of a body beneath the El Caliente dome using data from 76 events and also the relation between this behavior and observed activity at the surface.

BACKGROUND AND FIELD EXPERIMENT

Santiaguito grows within the crater formed by the 1902 Plinian eruption of its parent Santa María (Williams and Self, 1983). The locus of activity has migrated repeatedly since 1922, producing four distinct but overlapping domes (Rose, 1973). 'El Caliente' dome is the current source of a dacitic-andesitic lava flow and pyroclastic laden emissions, which occur on the order of every hour and are similar to the activity occurring since 1975 (SEAN v. 2(5)). Plumes typically rise to an altitude of 500 m – 1500 m above the vent and sporadically produce small pyroclastic flows.

A 5 station seismo-acoustic network was deployed around Santiaguito for 3.5 days from January 1st to January 4th 2009 local time (Figure 1). Sites were equipped with broadband seismometers and small acoustic arrays. Data from the three closest stations (CAL, CAM, DOM) are used in the majority of the analyses presented here due to their proximity to the source which gives a higher signal to noise ratio. CAL and CAM were outfitted with Güralp CMG 3ESP 60 s seismometers while DOM had a CMG 40T 30 s seismometer. They were located at 465 m, 957 m and 1086 m distance from the vent respectively. The 2 microphones at each site were built around All Sensors 1 inch differential pressure transducers with one pressure port blocked to allow signal to pass between ~40 s and the Nyquist frequency. All the instruments were connected to 24-bit REF TEK RT130 Data Acquisition Systems (DAS) with incoming data sampled at 100 Hz. Video was taken at 30 frames per second from SUM station while several other time-lapse cameras were operated along the edge of the Santa María crater.

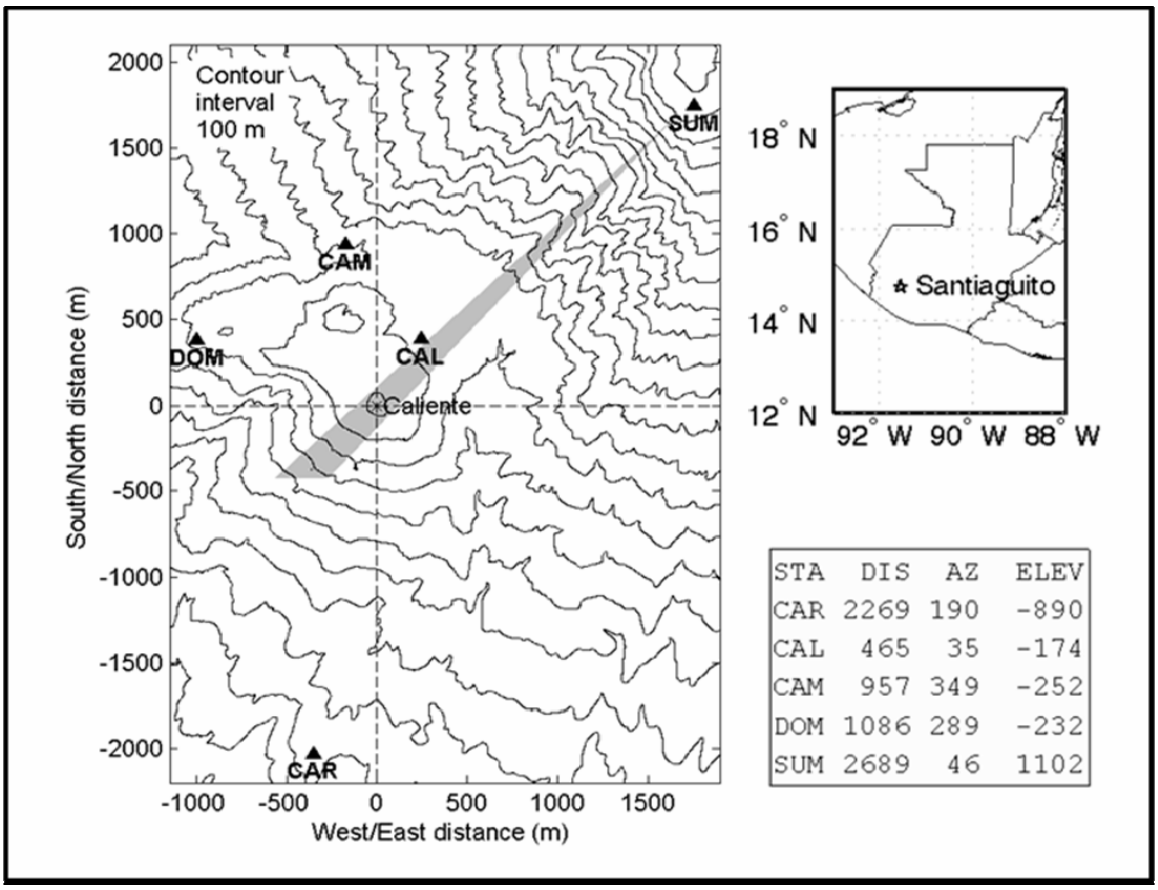

Figure 1: Topographic map of Santiaguito and Santa María with seismo-acoustic stations indicated. CAL, CAM, DOM and CAR all have seismo-acoustic sensors while SUM is acoustic only. The shaded area shows the vantage point used to record video and still images during the deployment. Regional map inset showing position of Santiaguito within Guatemala. The table gives the orientations, slant distances (m) and elevation differences (m) of the stations from the centre of the El Caliente vent.

SEISMO-ACOUSTIC AND VISUAL DATA

Eruptions and Degassing events

Two types of ULP signal are identified, those corresponding to eruptions and those corresponding to degassing events. ULPs, or Ultra-long Period events are seismic signals in the 600 – 30 s band. The term 'eruption' is defined here as extrusion of magma with vapor and/or pyroclastic emissions, which may include juvenile and recycled ash. Twenty five eruptions were observed on camera while 53 others were inferred from inspection of seismic records. In the 2009 catalogue, eruptions comprised 83% of events with ULP signal with degassing events associated with the remaining 17%. Figure 2 shows 24 hours of data comparing unfiltered and ULP signals. Notably, ULP events have variable amounts of associated higher frequency seismic signal. Following Johnson et al. (2009) these signals can be decomposed into Very-long Period (VLP, 30 to 5 s), Long Period (LP, 5 s to 1 s), Short Period (SP, 1 Hz to 10 Hz), and High Frequency (HF, 10 Hz to 50 Hz) bands. Figure 3 shows an eruption signal filtered into the aforementioned bands along with corresponding infrasound. Johnson et al. (2009) have broadly attributed these various high frequency seismic signals to various phenomena: response to pressurized gas flow, sub-vertical motion of the dome's upper surface, response to gas/pyroclastic emissions, fracturing of rock and/or ballistic impact from fallout and associated flows.

Based upon visual observations, SP seismic radiation during eruptions continues for the duration of the emission however subtle variations in those emissions correspond to a range of observed SP characteristics. The initial SP impulse is typically followed by

non-harmonic tremor (55%) or by harmonic tremor (33%). Some of the non-harmonic tremor episodes manifest as a clear sequence of rapidly repeating events. Tremor models invoking steady and unsteady gas flux through cracks (e.g. Kumagai and Chouet, 2000; Hellweg, 2000) are consistent with our observations though some post emission tremor may be explained by other means such as energy gradually leaking from within the conduit (Neuberg et al., 2000). Infrasound accompanies each eruption, tracking the SP seismicity envelope and containing a similar range of frequencies. Amplitudes up to 3.5 Pa were recorded at CAL. Although Sahetapy-Engel et al. (2008) reported extended plumes without any elastic energy being recorded, the noise levels and detection thresholds of the short period seismometer and electret condenser microphones were not specified in that study.

While emissions typically last 2 – 5 minutes in entirety (11 minutes maximum), the ULP signal continues for up to 15 minutes and is sensitive to signal processing (see Section 4). Inter-eruption repose times measured as the time between two successive even onsets range from 8 minutes to 3.5 hours with a mean of 71 minutes, standard deviation 38.5 minutes and skewness of 1.23. With regards to ULP derived pseudo-tilt (hereafter referred to just as 'tilt') at CAL, the maximum was 4.3 μrads, minimum 0.3 μrads, mean 1.6 μrads, standard deviation 1.0 μrads and skewness 0.92. Of the tilt signal waveforms, 76% are similar, comprised of a 75 – 150 s deflationary period followed by a minimum of a 75 – 225 s inflationary period. The remaining 24% of events show a secondary deflation while recovering from the first at a variable time delay following the first deflation and with varying magnitude. These supplemental deflations typically have

some associated SP manifestation (discussed in Section 6) No statistical relations between repose times and tilt amplitudes have been found.

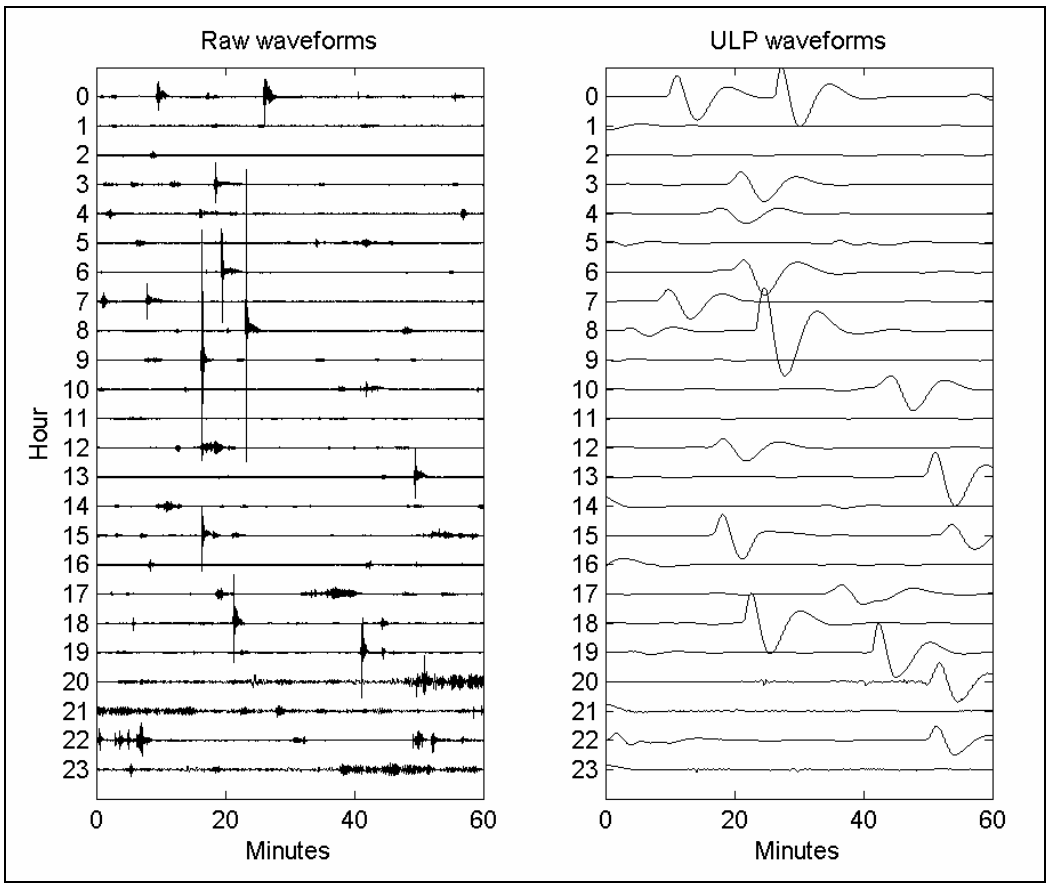

Figure 2: The left panel shows the raw radial seismic velocity recorded at CAL on January 3rd UTC. The record is dominated by SP energy associated with eruptions, rockfall and tremor. The right panel shows the same data but after it has been filtered, the instrument response removed, and then filtered again (Section 4). This process reveals the ULP energy hidden within the raw data. Notably SP energy and ULP energy are not uniformly present.

Degassing events are manifested by relatively low-amplitude and short-duration ULP signal in which a minimal amount of gas is released at a point on the vent margin and negligible SP and infrasound energy is present. During our field project 6 degassing events were visually observed while 10 others were inferred from seismic traces, making

up 17% of all ULP activity. Such events were also noted visually and thermally by Sahetapy-Engel et al. (2008) during observations in 2003, but they were not identified seismically due to potential instrumental limitations.

Both degassing and eruption events are indicated by clear ULP signal, but SP seismicity tends to be absent during non-explosive degassing events. The degassing event featured in Figure 4, for example, was observed as several minutes of fumarolic jetting with a vapor plume reaching only a few tens to hundreds of meters. Such low-vigor degassing doesn't appear to radiate substantial SP seismicity, but a ULP deflationary is nonetheless. Visual observations of the eruptions from Santa María summit are thus vital for understanding the origin of the ULP signals and how they are related to activity in the rest of the eruptive cycle.

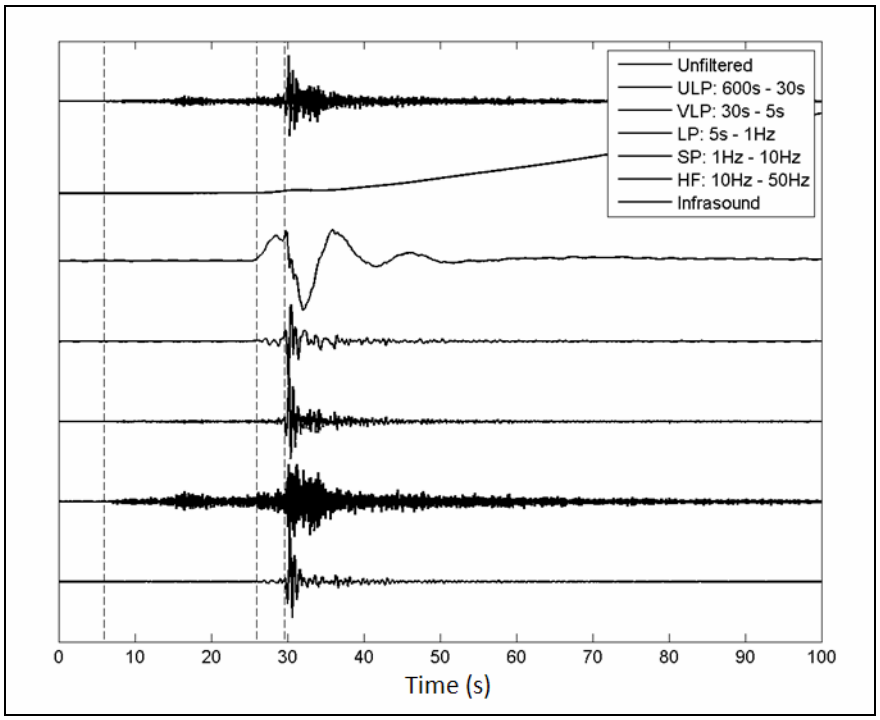

Figure 3: Typical eruption seismic signal at Santiaguito recorded at CAL and filtered into different frequency bands, plotted along with the infrasound trace filtered from 0.5 to

2 Hz. The seismic instrument response has been removed from each of the filtered events. Three dashed lines denote the initiation of different stages of the event. The first line, at 6 seconds, is the start of a rockfall that manifests only in the HF band. The second line marks the beginning of the 'precursory' seismicity phase where ULP, VLP, LP and HF energy is evident. The third line indicates the onset of the most seismically energetic part of the eruption, which is coincident with the primary infrasound signal and the onset of the explosive eruption seen at the surface.

Other seismic events

In addition to explosive eruptions and degassing events, several other types of earthquakes were recorded. Rock falls, associated with and also independent of eruptions, commonly descended the southwest flanks of Caliente. Many were detected across the seismic network. Tremor was also observed and did not always coincide with a visible eruption. Two prominent examples occurred during our study interval, each lasting for approximately 2 hours with spectral peaks at 0.05 and 0.06 Hz and relatively constant amplitude. These tremor episodes were accompanied by small amounts of gas released along the western edge of the vent though no ULP signals were observed. In addition to rock fall and tremor impulsive, low amplitude spectrally peaked events were recorded. Their duration of ~15 seconds and frequencies of 2 or 5 Hz resembled classical 'long-period events' that may reflect gas flux through an elastic crack (Chouet, 1996). Volcano-tectonic events, generated by brittle rock fracture (McNutt, 2005), were also observed and appeared to come from two depths. Deeper volcano tectonic events appeared as small amplitude and very impulsive signals with clear P and S wave arrivals. S-P time was on the order of 1 s, suggesting a depth of ~3 km. Shallower volcano tectonic events were more emergent and lacked distinct P and S arrivals but contained characteristic high frequencies (McNutt, 2005). At least seven volcano tectonic events were found.

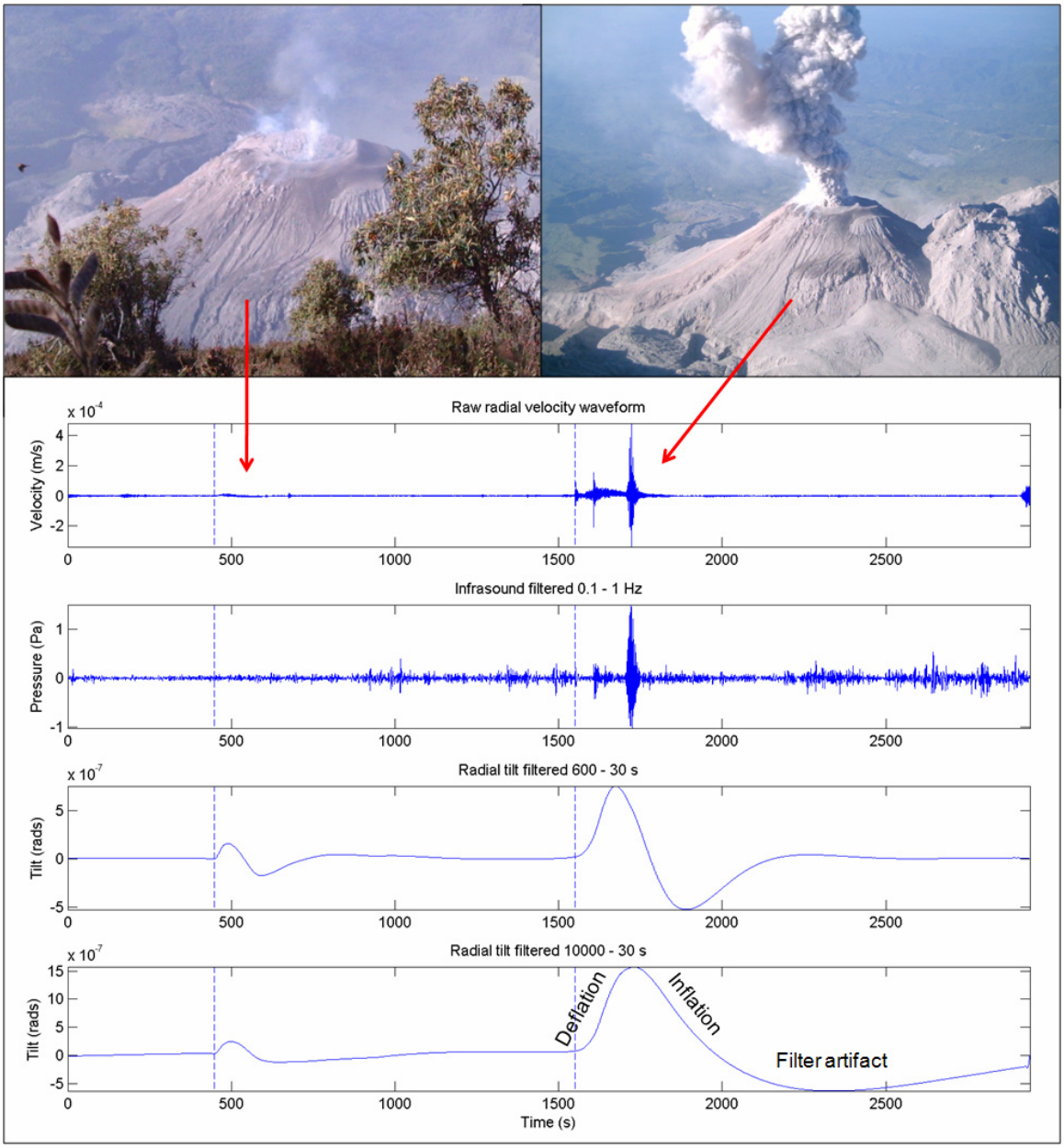

Figure 4: Comparison of the SP, ULP and visual manifestation of associated degassing events (left) and eruptions (right) beginning 1930 on January 1st 2009 UTC using data from CAL. While some ULPs occur with little surface activity or SP signals (such as the degassing event at left) most occur simultaneously with the ejection large amounts of gas and pyroclastics from the top of the dome and significant SP energy (eruptions). Dashed lines mark the onset of emissions for each of the events. View of Santiaguito is from Santa María.

SIGNAL PROCESSING

This study focuses on the repeating ULP signals because they are a key feature of Santiaguito degassing and eruption earthquakes. The vast majority of recorded ULP signals showed distinct radial and apparent horizontal outward motions that were recorded by the three closest seismometers. It is unlikely that these apparent motions correspond to outward radial translation given that the motions were recorded only on the horizontal channels and responsible long period displacements would be on the order of tens of cm. For these reasons the ULP is modeled as a tilt signal due to a deflating source that causes the seismometer to tilt towards the origin.

Tilt signals are recovered by first filtering the raw seismic velocity data using a 2-pole Butterworth minimum-phase IIR filter between 600 s and 30 s, consistent with Johnson et al., (2009). This frequency band was chosen as it is low enough that it reflects static rotational motions rather than dynamic motions inflicted by seismic waves, while not being so low that inherent instrument noise becomes inflated (Kinoshita, 2008). This filtering provides a band-limited record of tilt that illustrates Earth processes occurring down to about 10 minutes. For longer periods a dedicated biaxial tiltmeter would be beneficial. The IIR filter type was chosen for best overall performance after comparison with other IIR, FIR and all-pass filters with mixed-phase, zero-phase and minimum phase variants. While the chosen filter does induce phase artifacts to emerge in the latter part of the tilt waveform (Figure 5), compared to FIR filters, it is more efficient to implement and the wave onset is significantly less distorted by spurious oscillations. The latter point is important for interpreting the timing and subtleties of pre-eruptive seismicity.

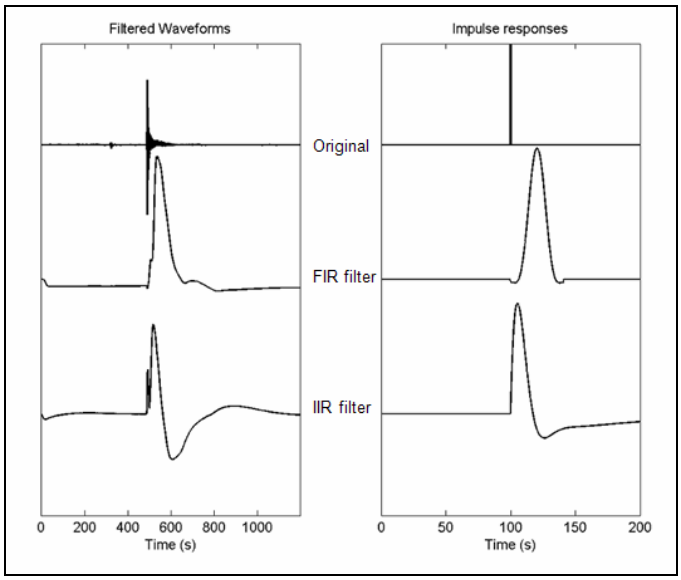

Figure 5: The choice of filter is critical to subsequent waveform evaluation and modeling. An unfiltered eruption velocity trace (upper left panel) is filtered with a 4096 pole FIR filter and with a 2 pole IIR filter between 600 and 30 s. The corresponding filter impulse responses are shown in the right hand panel.

After deconvolving the instrument response velocity seismograms are converted to tilt angle τ by taking the time time-derivative of the velocity trace v and dividing by the acceleration due to gravity g (Wielandt and Forbriger, 1999). The following show the relation between v and acceleration a where ü is the second derivative of dynamic displacement and t is time.

$$v = \int a \, dt = \int \ddot{u} - g\tau \, dt \qquad (1)$$

Translational contributions from ground accelerations $\ddot{u}$ are excluded by assuming that they are insignificant in the 600-30 s passband. This is evidenced by non-existent ULP signals on the vertical components, where tilt-induced ULP is effectively zero.

$$\tau = -\frac{1}{g}\frac{dv}{dt} \qquad (2)$$

Taking the time-derivative of a velocity seismogram (even one that is filtered) increases the high frequency energy so a final smoothing procedure is performed using a sliding mean filter (Figure 6 illustrates the entire digital signal process). Similar techniques that have been used to derive tilt from seismic data include those used by Kinoshita (2008), Wielandt and Forbriger (1999), Grazier (2006) and Aoyama and Oshima (2008).Local tilt fields caused by seismic strain-tilt coupling and site installation methods are a concern when dealing with such signals (Wielandt and Forbriger, 1999). Given the uncertainties associated with these effects noise amplitudes on each seismic channel (in the acceleration domain within the specified passband) are analysed to recover local site effects. Based upon non-volcano source amplitudes the following weighting factors were applied to the ULP data for the CAL, CAM and DOM East and West components respectively: [0.74, 0.64], [0.82, 0.88] and [0.30, 0.21]. This type of site correction led to tighter clustering of locations as shown in Sections 5.1 and 5.2. Considering the ultra-long periods being considered with respect to the network aperture, it may be that the apparent in addition to the above factors differences in site and channel response are due to low-frequency instrument response deviations from manufacturer's specifications.

Broad band seismometers are unable to measure static changes, i.e. down to DC, but decent signal is often recoverable at frequencies many octaves below the specified lower corner frequency of the instrument. Given the right conditions however motions with periods of up to at least 25000 s can be detected and analyzed (Wiens et al., 2005). Although data was filtered from 600-30 s for tilt analysis a spectral peak in velocity seismograms was noted that is as long as ~3000 s on the nearest station, CAL (see Figure

4). This velocity seismogram signal corresponds to a ~400 s deflation followed by a ~1000 recovery, or inflation. The amplitudes of the 3000 s period signals are 4 times those when filtered at 600 – 30s having a consequence for modeling source mechanisms. Unfortunately, the 3000 s signal appears to be noisy on the more distant stations, CAM and DOM, and prevents it being used in source strength inversions (see Section 5). Due to this issue the first half-period of the filtered (600 – 30 s) signals are focused upon, which reflects a relatively quick deflationary process. Quasi static tilts and/or very slow inflationary processes, which follow the deflationary signal are not well recorded by our seismic network and are thus beyond the scope of this paper.

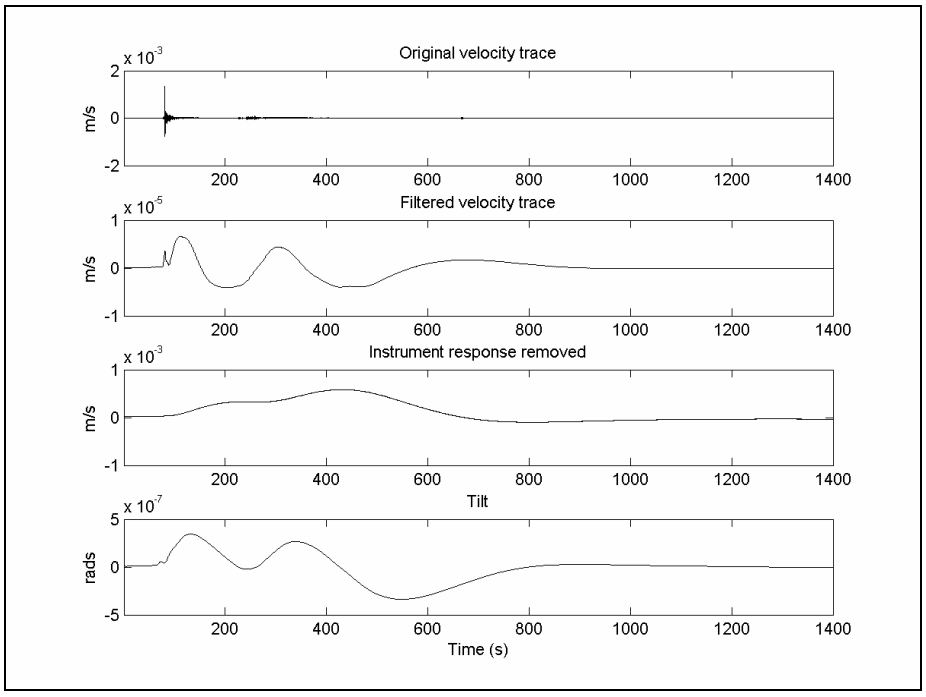

Figure 6: Conversion of recorded CAL velocity trace (top trace) into tilt record (bottom trace). Raw trace is filtered to the 600-30 s passband then instrument response is removed. Finally the time derivative is taken and the waveform is scaled by *g*. Tilt convention is that upward polarity indicates downward tilt towards the source (deflation). This particularly event from 0738 on January 2nd UTC shows an additional deflation after the first cycle. Both deflationary pulses coincide with SP energy.

ULP SOURCE MODELS

ULP signals recorded at CAL, CAM, and DOM are used to find both the position and the strength of a Mogi-type volumetric source associated with eruptions and degassing. This first-order inversion uses 6 tilt components at three stations to solve for 4 unknown quantities associated with a spherical isotropic volume change. Seismograms from further stations, such as from CAR, at a distance of 2.3 km to the south cannot be used, because it did not record any ULP tilt, even for the largest event. The absence of tilt on these further stations is due to the rapid fall off of the elastostatic wavefield and also, potentially, to the fact that CAR is located below the located source and should therefore experience a smaller degree of tilt.

Hodograms

Hodograms were used to determine a 2D source location around which can be built a search grid for a subsequent Mogi source inversion. The particle motion of the tilt for all 3 stations are plotted along with back azimuths determined through principle component analysis (Figure 7). Preliminary 2D source locations are then determined by finding the center of the triangle formed by the three intersecting back azimuths. Of the 76 eruptions, 44 had sufficient signal-to-noise levels on all 3 stations such that they could be located approximately. Locations are clustered and offset ~150 m to the northwest from the summit and vent area of El Caliente. Interestingly, these locations coincide with the centre of effusion during 1986-1990 (Harris et al., 2003). Only those eruptive events

with signal-to-noise ratios sufficient to be located using the hodogram method were considered for subsequent modeling.

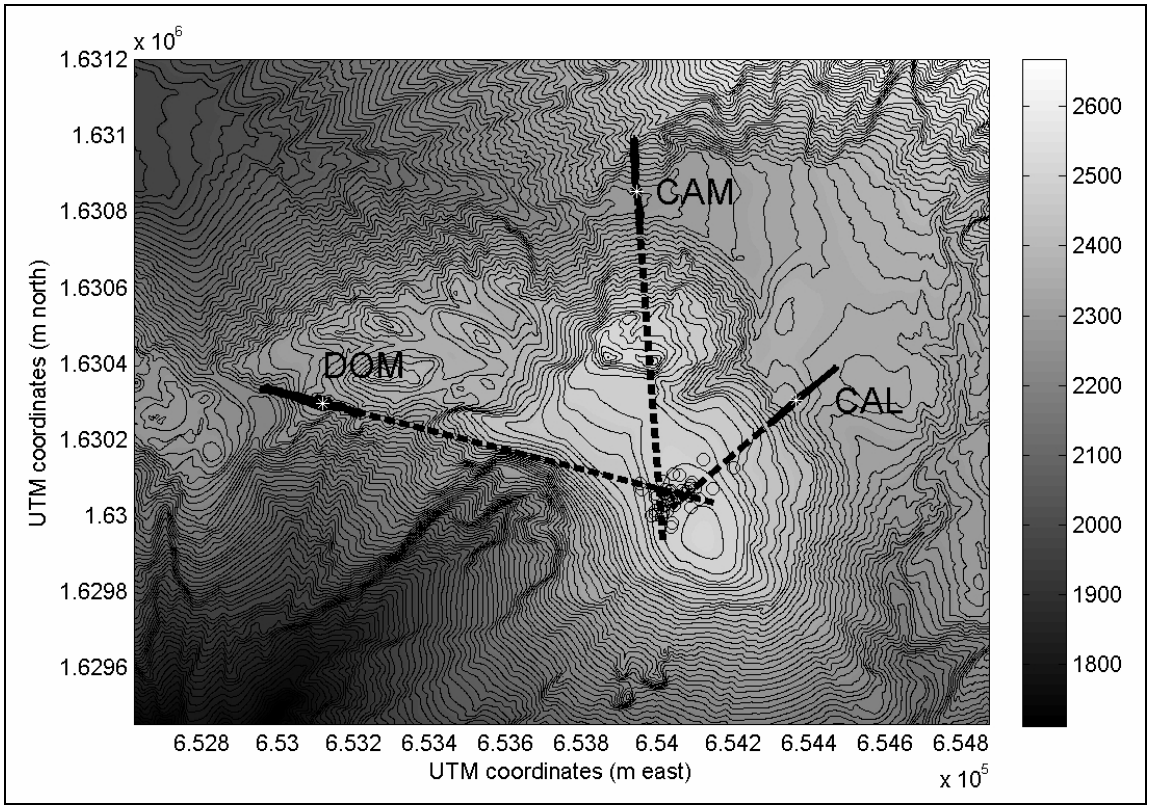

Figure 7: Hodogram plot (black traces) and principal components (dashed black lines) point toward an inferred 2D volumetric source for an event occurring at 0503 on January 2nd UTC. Locations for other events shown as black circles. Topographic map has contours at 10 m intervals (JICA et al., 2003). Relative hodogram scales have been adjusted for ease of viewing.

Spherical body (Mogi) modeling

A variety of methods and model types have been used to model surface tilt and deformation at volcanoes (Tiampo et al., 2000; Kawakatsu et al., 2000; Ohminato and Chouet, 1997; Costa et al., 2007). Due to the limited number of tilt measurements at Santiaguito a Mogi source (Mogi, 1958) was solved for using a grid search. Despite the

simplistic nature of an isotropic volumetric source (e.g. McTigue, 1987), the Mogi inversion is commonly used and provides a convenient metric of relative pressurization or depressurization (e.g. Tiampo et al., 2000). At Santiaguito it provides a means to compare relative locations and strengths for a suite of eruptive events.

The grid search for a Mogi source at Santiaguito found a minimum residual by comparing the observed EW and NS tilt vector amplitudes at CAL, CAM and DOM with the synthetic tilt amplitudes associated with a Mogi source (after Aster et al., 2003):

$$\theta_r = \frac{-9\Delta V}{4\pi} \frac{r z_0}{(r^2 + z_0^2)^{3/2}} \tag{3}$$

$$\theta_x = \frac{-9\Delta V}{4\pi} \frac{x z_0}{(r^2 + z_0^2)^{3/2}} \tag{4}$$

$$\theta_y = \frac{-9\Delta V}{4\pi} \frac{y z_0}{(r^2 + z_0^2)^{3/2}} \tag{5}$$

where Θ is the maximum radial tilt observed, ΔV maximum volume change, x, y, and r are eastward, northward and radial distance along the surface and z_0 is depth to the Mogi source. The free parameters used in the grid search are the three positional coordinates and the maximum change in volume, or the source strength. The spatial grid spacing was 25 m and comprised a search volume 600 m by 600 m in horizontal extent and ranging from 0 m elevation (relative to CAL) down to 1 km depth. Source strength was varied in 25 m^3 increments up to a volume change of 3000 m^3. The root mean square statistic was used as the measure to assess residual size. The results of the grid search are shown in Figure 8 for the 44 locatable events; Figure 8a shows plan view locations of Mogi sources along with modeled and observed tilt vectors for an individual event. Figure 8b provides a map of 3D hypocenters. The source region appears to be for the most part clustered in a 75 m x 100 m horizontal x 25 m thick volume. Volume changes for the

suite of events ranged from 125 to 1825 m^3 and did not appear strongly dependent upon depth (Figure 8c). In general tilt amplitudes appear to be far more sensitive to inherent volume change rather than vertical position within the edifice.

In terms of goodness of fit, CAL vectors are fit exactly while CAM vectors show a 7% overshoot in the dominant north direction while DOM's dominant eastward vector is underestimated by 10%. These errors are not surprising considering the generally diminished signal-to-noise at CAM and DOM. Without the imposed site correction, fits would have been significantly poorer at CAM.

Misfit could also certainly be due to the assumption of an isotropic point source (Mogi, 1958). More complicated source geometries might fit the ULP-derived tilt data more satisfactorily, such as dikes and cracks (e.g., Costa et al., 2007; Okada, 1985). Unfortunately with our limited observations of biaxial tilt at three stations it is not possible to adequately constrain even a point source crack, which would have precisely 6 degrees of freedom (3 position, 2 orientation, and 1 strength). Attempts to fit the data with a vertical point source crack found inferior fits compared to the Mogi source model.

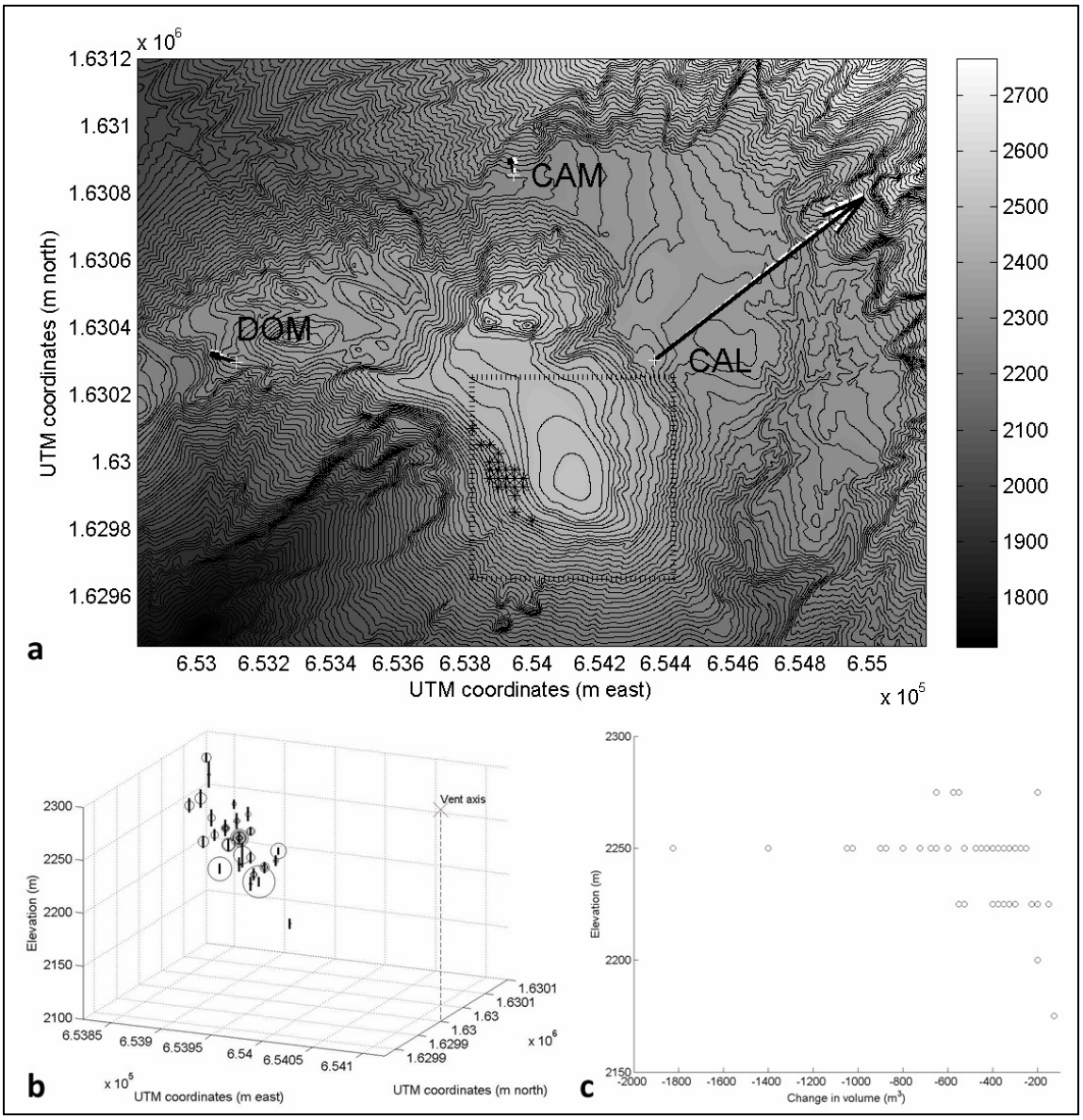

Figure 8: (a) 44 located Mogi sources (asterisks) shown in plan view. Black square indicates extent of grid search region. Observed tilt vector data from a representative event at 1119 on January 4th UTC are shown in black with modeled best fit data in white. (b) Mogi sources shown in three dimensions with circle size proportional to inferred volume change. Bar length is proportional to RMS residual and is inversely proportional to goodness of fit. (c) Plot of inferred volume change versus depth for each of the events.

DISCUSSION

Although there is some ambiguity over the precise geometry of the volumetric source the best fit results for Mogi and vertical crack point sources both put the source region about 150 – 200 m West or Northwest of the Caliente summit and ~250 - 275 m below the 2500 m elevation summit vents. Equivalent volume loss responsible for the tilt signals is on the order of 10^2 to 10^3 m^3. These volume losses occur regularly and are associated both with explosive eruptions and passive degassing and it is sensible that the edifice is responding to an outflux of gas or condensed phase material. Additional constraints on the eruptive mechanisms may be inferred by examination of waveforms. Relative timing between the onsets of different phases and their durations are of particular interest.

The majority of seismic signals associated with eruptions involve a strong impulse that corresponds to the onset of the visual part of the eruption itself. This impulse is typically preceded by 5-10 s of seismicity that is present across all frequency bands (Figure 3). Following this energy in all bands, with the exception of the ULP, appears more or less simultaneously. For example, precursory HF band energy, which was previously attributed to ballistic fallout or rock fall (Johnson et al., 2009), may indicate fracturing phenomena within the dome. The broadband signals generated by such processes would also carry over to the SP band, which is often attributed to the onset of eruptive degassing at the surface. It is proposed that precursory energy in the LP band and the lower part of the SP band may be related to gas accumulating beneath a proposed 'lava pad'. Although Johnson et al. (2008) did not note any dramatic surface dome uplift

during the precursory phase, Doppler radar measurements suggest that some slow preliminary uplift might occur (Scharff et al., 2009). Gross waveform shape and spectral properties of precursory seismicity recorded at Santiaguito in January 2007 were not found to be related to properties of the co-eruptive seismicity; neither the duration nor amplitude of the precursory events were predictors of the subsequent explosion.

Comparison of ULP-inferred tilt and the SP seismicity associated with eruption an eruption event showed a large degree of variation in amplitude ratio and temporal relation. From the 76 classified eruptions, 39 indicated precursory deflation occurring as much as 60 s (more typically up to 10 s) before emissions began while 5 eruptions indicated emissions (i.e., SP pulses) beginning prior to deflation. Twenty five events showed deflation beginning near simultaneously with emissions while 10 events showed both minor precursory emissions and deflation prior to the main deflation/inflation episode. As described in Section 3.1, 13 events involved a relatively small deflation/inflation cycle superimposed on a primary deflation. An additional 5 of these smaller sub-events events showed no emissions despite a clear ULP pulse. These items are addressed further in Section 7 within the context of a general model.

Following an eruptive event featured by Johnson et al. (2009) it is found that vigorous degassing (as inferred from high amplitude infrasound) terminates prior to the time when deflation transitions to deflation. This suggests gas venting is directly related to edifice deflation and that inflation only resumes when the conduit system seals itself during the inter-eruption quiescent interval. A similar observation was retrospectively found for ULPs in 2007 during a season when both ULP inflation and emissions were shorter.

ULP and SP energies were compared to plume growth rates when digital video images were available. A qualitative gas flux proxy was estimated from the duration of emissions, muzzle velocity (as seen with video) and maximum plume volume as extracted from video still images. While a positive correlation was found for ULP and plume growth, no similar relation was discernible for SP events. These observations are explained if ULP energy is proportional to cumulative gas flux erupted through the system during each eruption whereas SP seismicity is related to the specific force imparted during a thrust response of the volcanic edifice. This finding suggests that plume character or eruption 'size' cannot be directly estimated from SP seismic records In the future it would be beneficial to more carefully compare inferred edifice volume deflation with quantified plume volume emissions, such as determined by Yamamoto et al. (2008) using ultraviolet imagers.

Inferred cumulative volume flux (i.e. of gas and/or magma), as measured in the 600-30 s band, appears relatively constant over daily scales, but is somewhat variable on hourly scales (Figure 9). The average volume loss, calculated by integrating the volume deflation phase only, was ~ 6170 m^3 of material per day. If this volume flux represented a fluid magma effusion, it would be comparable to reported lava flow fluxes of 7500 m^3 / day (BGVN 15(11)) and also to projected trends for 2009 found by extrapolating the historical trends detailed by Harris et al. (2003). Alternatively the cumulative deflation volumes might represent integrated gas evacuation events. This scenario is considered most likely as the surface lava extrusion appears to be a continuous process while the gas emissions occur episodically and concurrently with visual observations of eruptions or degassing.

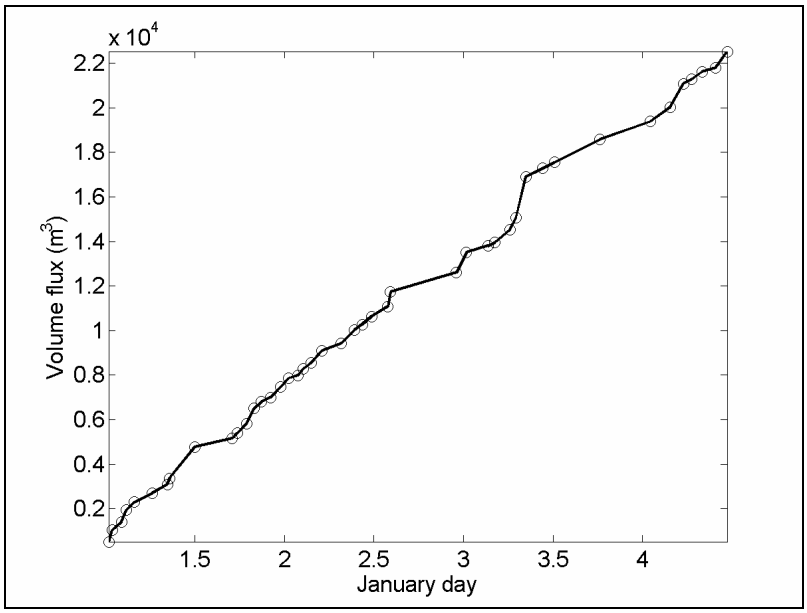

Figure 9: The cumulative flux of material estimated using the Mogi model results are plotted here over time. There is a clear approximate linear trend over the course of the 3.5 days with some minor variation at shorter timescales. The mean flux indicated over this time period was 6170 m^3/day though this amount varies depending on the passband used.

MODEL OF ERUPTIVE CYCLE

Repeated eruptive cycles are observed, which lasted about 1 hour in 2009, involve 3 main stages. These stages are: the pre-eruptive period (lasting for up to a minute prior to an eruption), the eruptive period (lasting for 1-11 minutes while there are visible pyrolcastic emissions) and the inter-eruptive period (lasting from the end of degassing to the next pre-eruptive phase). Each of these stages is conceptually described below, assuming that the dome is acting as a plug within a flared vent region sitting atop a non-vertical 'upper- conduit' that extends to depth. The cyclical behaviour is based upon stick-slip motion of the plug (Sahetapy-Engel, 2008; Bluth and Rose, 2004) such as was applied to Mount St. Helens during the 2004 sequence (Iverson et al., 2006). A constant magma supply rate inducing pressurization at depth has been shown to maintain this type of episodic activity (Denlinger and Hoblitt, 1999).

Pre-eruptive period

Gas steadily accumulates beneath the annealed carapace of the dome during the inter-eruptive period via the relatively slow process of exsolution (Proussevitch & Sahagian, 1996). As exsolved gases accumulate, the dome remains largely static as internal pressures rise beyond magmastatic pressures. The magma plug eventually overcomes friction and begins to slip due to building gas and deep conduit pressure (Wylie et al., 1999). As strain increases fractures coalesce (Tuffen et al., 2008) increasing gas mobility in the upper conduit. The movement of fluid magma, separated gas phases, and resultant fracturing events are all likely sources of the broadband precursory

seismicity that is seen in the pre-eruptive interval. While not always observed, some precursory seismicity lasts several minutes and involves small ash-puffs or jetting (Sahetapy-Engel et al., 2008; Johnson et al., 2009), suggesting an open conduit system reaching all the way to the surface.

Eruptive period

Accumulating pressurization beneath a largely immobile plug finally induces motion of the plug as shear stresses exceed the shear strength of the boundary between the plug and wall rock. The plug moves upwards and outwards (Denlinger and Hoblitt, 1999) and 'drags' the upper surface of the dome with it as seen by Johnson et al. (2008) with particle image velocimetry techniques that were correlated with long period seismicity. In the case of the Johnson et al. (2008) study they treated the dome surface as a cohesive lava carapace atop a region of pressurized gas existing as a separated phase. As the dome is abruptly strained it breaks along arcuate/ring fractures that develop on the surface and around the centre of the plug (Bluth and Rose, 2004; Massol and Jaupart, 2009). The gas release and abrupt acceleration of the plug generates an infrasound and broadband seismic response.

Vigorous degassing bleeds the gas overpressure until the surface collapse and fractures close, a process which generally lasts no more than 75-150 s (Section 3.1). Coincidentally ULP-derived tilt deflation is observed. Occasionally, small deflation-inflation cycles are seen on top of the main ULP tilt waveform indicating that gas evacuation sub-events may trigger one another (e.g. Iguchi et al., 2008) or that material is entering the upper-conduit from depth during the eruption and then leaving again.

Deflation amplitudes and rates are quite variable (Figure 8) and there is a lack of correlation between inter-eruptive repose times and deflation amplitudes. This contrasts with the generally self-similar and longer period pressurization cycles seen, for example, at Soufrière Hills (Green et al., 2006).

ULP-derived deflation is apparent for all explosive eruptions and tends to begin coincidentally with the onset of explosive degassing and high-amplitude broadband seismic radiation. It is notable that the inferred depressurization source centroids, determined either through Mogi or vertical crack source models, are consistently located at 250 – 275 m below the Caliente summit vents. These depths suggest that during eruption a gas volume reservoir at significant depth is depleted as gas travels through an interconnected system of cracks. Although the geometry of the depressurizing source is certainly more complicated than a sphere or point source crack, it is maintained that a depressurizing volume, be it cracks, conduit, or spheroids, extends down to pressures of at least 7 MPa (magmastatic pressure at 250 - 275 m). It is significant that Santiaguito eruptions are able to tap gas reservoirs down to this depth during their hourly episodic eruptions. This location may be at the base of the plug if the minimum plug extent of 100 – 250 m depth inferred by Sahetapy-Engel et al. (2008) is considered.

Inter-eruptive period

Edifice deflation that occurs during the co-eruptive period must be balanced by a re-inflation that occurs largely during the inter-eruptive period. Otherwise successive eruptions would contribute to a cumulative volume loss of the edifice, which has not been observed at Santiaguito over months and years. It is speculated that inflation begins with

the effective annealing of the upper conduit system cracks and continues until the carapace is again disrupted. Inflation is caused due to slow processes such as gas diffusion from the fluid magma into existing gas vesicles. Occasionally an inter-eruptive period will be interrupted by a degassing event, in which a system of cracks opens sufficiently to allow gas flow to the surface. These degassing events are associated with volume loss and edifice deflation, but they do not result in very explosive degassing, rapid dome uplift, and/or brittle failure in the conduit, all of which may be associated with LP, SP, and HF seismicity.

Future work

Future study at Santiaguito would benefit from a greater distribution of seismometers at a range of azimuths and distances around the Caliente vent. This would enable a more detailed inversion of the responsible volumetric ULP source ad could discriminate between spheroidal, crack, and finite-dimension sources. In addition, future work will benefit from dedicated tilt meters, which measure tilt down to DC. It would be particularly beneficial to recover the accurate time history of the hour-long inflationary process, which is well below the response of our seismometers, as well as the deflationary process. Tilt meters and rotational seismometers should be co-located with typical broadband seismometers to validate results using our methods (e.g. Battaglia et al., 2000) and/or installed permanently to act as a pressure meter to provide warning against potential dome collapses.

CONCLUSIONS

Interpretation of seismicity and infrasound generated prior to, during and between eruptions can be used in the context of a system model to understand the complex physical processes going on at the surface and inside Santiaguito. The seismic record from Santiaguito allows us to identify three characteristic phases of the cyclic eruptive sequence, which lasted from 1-2 hours in January of 2009. These repeating phases include a quiescent recharge interval, in which the conduit becomes pressurized, followed by a short pre-eruption conduit failure process, and finally the eruption event itself. Pseudo-tilt signals inferred from a network of three seismic stations detect deflation of a shallow (250 – 275 m) conduit source occurring on a time scale on the order of minutes. This deflation is coincident with the onset of the eruption. A corresponding re-inflation, which presumably occurs more slowly during the inter-eruptive interval, is largely below the detection threshold of our 30-60 s semi-broadband seismometers. Although our deflation source inversion cannot definitively discriminate between different geometries, it has been possible to assess their relative magnitudes as equivalent volume losses, which range from hundreds to thousands of cubic meters for a suite of 44 explosions. Such deflations occur coincidentally with visible gas emissions at the surface that occur both as an explosive eruption and as more passive degassing. The more passive degassing events are accompanied by ULP-inferred deflation, but have very little SP or LP seismic manifestation. It is speculated that these less vigorous emissions do not impart significant force to the volcanic edifice.

REFERENCES

Amelung, F., Jonsson, S., Zebker, H., Segall, P., 2000. Widespread uplift and 'trapdoor' faulting on Galapagos volcanoes observed with radar interferometry. Nature. 407, 993-996.

Aoyama, H., Oshima, H., 2008. Tilt change recorded by broadband seismometer prior to small phreatic explosion of Meakan-dake volcano, Hokkaido, Japan. Geophys. Res. Lett. 35, L06307, doi:10.1029/2007GL032988.

Aster, R, Mah, S., Kyle, P., McIntosh, W., Dunbar, N., Johnson, J., Ruiz, M., McNamara, S., 2003. Very long period oscillations of Mount Erebus Volcano. J. Geophys. Res. 108, B11, 2522, doi:10.1029/2002JB002101.

Barmin A., Melnik O., Sparks R.S.J., 2002. Periodic behavior in lava dome eruptions. Earth Planet. Sc. Lett.. 199, 173-184.

Battaglia, J., Aki, K., Montagner, J. -P., 2000. Tilt signals derived from a GEOSCOPE VBB Station on the Piton de la Fournaise Volcano. Geophys. Res. Lett. 27(5), 605–608.

Bluth, G.J.S., Rose, W.I., 2004. Observations of eruptive activity at Santiaguito volcano, Guatemala. J. Volcanol. Geoth. Res. 136, 297-302.

BGVN, Smithsonian Institution, Global Volcanism Network Bulletins.

Chouet, B.A., 1996. Long-period volcano seismicity: its source and use in eruption forecasting. Nature. 380, 309–316.

Costa, A., Melnik, O., Sparks, R.S.J., Voight, B., 2007. Control of magma flow in dykes on cyclic lava dome extrusion. Geophys. Res. Lett. 34, L02303, doi:10.1029/2006GL027466.

Denlinger, R.P., Hoblitt, R.P., 1999. Cyclic eruptive behavior of silicic volcanoes. Geology. 27, 459-462.

Gonnermann, H.M., Manga, M., 2003. Explosive volcanism may not be an inevitable consequence of magma fragmentation. Nature. 426, 432-435.

Grazier, V., 2006. Tilts in strong ground motion. B. Seismol. Soc. Am. 96, 2090-2102.

Green, D. N., Neuberg, J., Cayol, V., 2006. Shear stress along the conduit wall as a plausible source of tilt at Soufrière Hills volcano, Montserrat. Geophys. Res. Lett. 33, L10306, doi:10.1029/2006GL025890.

Harris, A.J.L., Rose, W.I., Flynn, L.P., 2003. Temporal trends in lava dome extrusion at Santiaguito, 1922-2000. B. Volcanol. 65, 77-89.

Hellweg, M., 2000. Physical models for the source of Lascar's harmonic tremor. J. Volcanol. Geoth. Res. 101, 183-198.

Iguchi, M., Yakiwara, H., Tameguri, T., Hendrasto, M., Hirabayashi, J., 2008. Mechanism of explosive eruption revealed by geophysical observations at the Sakurajima, Suwanosejima and Semeru volcanoes. J. Volcanol. Geoth. Res. 178, 1-9.

Iverson, R.M., Dzurisin, D., Gardner, C.A., Gerlach, T.M., LaHusen, R.G., Lisowski, M.L., Major, J.J., Malone, S.D., Messerich, J.A., Moran, S.C., Pallister, J.S., Qamar,

A.I., Schilling, S.P. and Vallance, J.W., 2006. Dynamics of seismogenic volcanic extrusion at Mount St Helens in 2004–05. Nature. 444, 439-443.

Japanese International Development Agency (JICA), Instituto Geografico Nacional (IGN), Instituto Nacional de Sismologia, Vulcanologia, Meteorologia e Hidrologia (INSIVUMEH), and Secretaria de Planificacion y Programacion de la Presidencia (SEGEPLAN), 2003. Estudio del establecimiento de los mapas basicos y mapas de amenaza para el sistema de informacion geografica de la Republica de Guatemala. Final Report.

Johnson, J.B., Harris, A.J.L., Sahetepy-Engel, S.T.M., Wolf, R., Rose, W.I., 2004. Explosion dynamics of pyroclastic eruptions at Santiaguito Volcano. Geophys. Res. Lett. 31, L06610, doi:10.1029/2003GL019079.

Johnson, J.B., Lees, J.M., Gerst, A., Sahagian, D., Varley, N., 2008. Long-period earthquakes and co-eruptive dome inflation seen with particle image velocimetry. Nature. 456, 377-381.

Johnson, J. B., Sanderson, R., Lyons, J., Escobar-Wolf, R., Waite, G., Lees, J.M., 2009. Dissection of a composite volcanic earthquake at Santiaguito, Guatemala. Geophys. Res. Lett. 36, L16308, doi:10.1029/2009GL039370.

Kawakatsu, H., Kaneshima, S., Matsubayashi, H., Ohminato, T., Sudo, Y., Tsutsui, T., Uhira, K., Yamasato, H., Ito, H., Legrand, D., 2000. Aso94: Aso seismic observation with broadband instruments. J. Volcanol. Geoth. Res. 101, 129-154.

Kinoshita, S., 2008.Tilt Measurement Using Broadband Velocity Seismograms. B. Seismol. Soc. Am. 98, 1887-1897.

Kumagai, H., Chouet, B.A., 2000. Acoustic properties of a crack containing magmatic or hydrothermal fluids. J. Geophys. Res. 105, B11, 25493-25512.

Massol, H., Jaupart, C., 2009. Dynamics of magma flow near the vent: Implications for dome eruptions. Earth Planet. Sc. Lett. 279, 185-196.

McNutt, S.R., 2005. Volcano Seismology, Annu. Rev. Earth Pl. Sc. 33, 461-491.

McTigue, D.F., 1987. Elastic stress and deformation near a finite spherical magma body: resolution of the point source paradox. J. Geophys. Res. 92, B12, 12, 931-12, 940.

Mogi, K., 1958. Relations between the eruptions of various volcanoes and the deformations of the ground surface around them. B. Earthq. Res. I. Tokyo. 36, 99-134.

Neuberg, J., Luckett, R., Baptie, B., Olsen, K., 2000. Models of tremor and low-frequency earthquake swarms on Montserrat. J. Volcanol. Geoth. Res. 101, 1-2, 83-104.

Ohminato, T., Chouet, B.A., 1997. A free-surface boundary condition for including 3D topography in the finite-difference method. B. Seismol. Soc. Am. 87, 494-515.

Okada, Y., 1985. Surface deformation due to shear and tensile faults in a half-space. B. Seismol. Soc. Am. 75(4), 1135-1154.

Proussevitch, A.A., Sahagian, D.L., 1996. Dynamics of coupled diffusive and decompressive bubble growth in magmatic systems. J. Geophys. Res. 101, 17,447-17,156.

Rose, W.I., 1973. Pattern and Mechanism of Volcanic Activity at the Santiaguito Volcanic Dome, Guatemala. Bull. Volcanol. 37, 73-94.

Sahetapy-Engel, S.T., Harris, A.J.L., Marchetti, E., 2008. Thermal, seismic and infrasound observations of persistent explosive activity and conduit dynamics at Santiaguito lava dome, Guatemala. J. Volcanol. Geoth. Res. 173, 1-14,

Scharff, L., Hasenclever, J., Hort, M.K., 2009. Oscillating dome at Santiaguito? A numerical model to explain inter-eruptive pulses. EOS Trans. AGU. 90(52), Fall Meet. Suppl., Abstract V23D-2146.

SEAN, Smithsonian Institution, Scientific Event Alert Network bulletins.

Tiampo, K.F., Rundle, J.B., Fernández, J., Langbein, J., 2000. Spherical and ellipsoidal volcanic sources at Long Valley Caldera, California, using a genetic algorithm inversion technique. J. Volcanol. Geoth. Res. 102, 189-206.

Tuffen, H., Smith, R., Sammonds., P.R., 2008. Evidence for seismogenic fracture of silicic magma. Nature. 453, 511-514.

Voight B., Young K.D., Hidayat D., Subandrio; Purbawinata M.A., Ratdomopurbo A., Suharna, Panut, Sayudi D.S., LaHusen R., Marso J., Murray T.L., Dejean M., Iguchi M., Ishihara K., 2000. Deformation and seismic precursors to dome-collapse and fountain-collapse nuees ardentes at Merapi Volcano, Java, Indonesia, 1994-1998. Journal of Volcanology and Geothermal Research. 100, 261-287.

Wielandt, E., Forbriger, T., 1999. Near-field seismic displacement and tilt associated with the explosive activity of Stromboli. Ann. Geof. 42(3), 407-416.

Wiens, D. A., Pozgay, S.H., Shore, P.J., Sauter, A.W., White, R.A., 2005. Tilt recorded by a portable broadband seismograph: The 2003 eruption of Anatahan Volcano, Mariana Islands. Geophys. Res. Lett. 32, L18305, doi:10.1029/2005GL023369.

Williams, S.N., Self, S., 1983. The October 1902 Plinian eruptions of Santa María volcano, Guatemala. J. Volcanol. Geoth. Res. 16, 33-56.

Wylie, J.J., Voight, B., Whitehead, J.A., 1999. Instability of Magma Flow from Volatile-Dependent Viscosity. Science. 285, 1883-1885.

Yamamoto, H., Watson, I.M., Phillips, J.C., Bluth, G.J., 2008. Rise dynamics and relative ash distribution in vulcanian eruption plumes at Santiaguito Volcano, Guatemala, revealed using an ultraviolet imaging camera. Geophys. Res. Lett., 35, L08314, doi:10.1029/2007GL032008.